ORGANIC CHEMISTRY

Rhodium-catalyzed atropodivergent hydroamination of alkynes by leveraging two potential enantiodetermining steps

Ruijie Mi[1], Rongkai Wu[2], Jierui Jing[3], Fen Wang[3], Xiao-Xi Li[1], Xin Hong[2,4,5]*, Xingwei Li[1,3]*

A pair of enantiomers is known to have different biological activities. Two catalysts with opposite chirality are nearly always required to deliver both enantiomeric products. In this work, chiral rhodium(III) cyclopentadienyl complexes are repurposed as efficient catalysts for enantiodivergent and atroposelective hydroamination of sterically hindered alkynes. Products with opposite chirality have been both obtained using the same or closely analogous chiral catalyst in good efficiency and excellent enantioselectivity, and the enantiodivergence was mainly enabled by an achiral carboxylic acid and its silver salt. Mechanistic studies revealed the origin of the enantiodivergence ascribable to the switch of the enantiodetermining step (alkyne insertion versus protonolysis) under acid control, which constitutes a previously unidentified working mode of enantiodivergence by leveraging two elementary steps.

INTRODUCTION

The design of chiral catalysts that accommodate various elementary steps and stabilize corresponding intermediates has been long sought in asymmetric catalysis. In this context, chiral cyclopentadienyl complexes of rhodium and iridium [Cp^XRh(III) and Cp^XIr(III)] stand out as powerful catalysts in asymmetric activation of C─H bonds (*1*–*13*), as pioneered by Cramer and co-workers and notably contributed by You and others (*14*–*21*). These catalysts typically undergo cyclometalation, and the organorhodium intermediate interacts with an unsaturated reagent to continue the catalytic cycle. Alternatively, analogous organorhodium intermediates were accessible via transmetalation (*22*–*24*) or alkyne cyclization (Fig. 1A) (*25*). Overall, these systems take advantage of the innate reactivity of soft Rh─C bonds. In contrast, Rh(III)─N bonds with a hard nitrogen ligand such as amine/amide have been rarely explored in catalysis, likely due to their intrinsically low reactivity toward migratory insertion. Recently, Ellman and others have realized rare systems of Rh(III)/Ir(III)-catalyzed N─H insertion into carbene reagents (*26*, *27*). However, these studies are limited to racemic or achiral reactions, and only a few Rh(III)-catalyzed asymmetric systems other than C─H activation have been realized, such as oxyamination (*28*) and olefin aziridination (*29*, *30*).

Asymmetric hydroamination has received increasing attention as an atom-economic approach toward the construction of chiral amines (*31*–*36*). Still, asymmetric hydroamination has been predominantly limited to creation of central chirality. Hartwig, Hou, Breit, Dong, and others (*37*–*44*) explored asymmetric hydroamination of diverse olefins. Meanwhile, catalytic asymmetric hydroamination of carbene reagents provides an alternative approach (*45*–*55*). In contrast, atroposelective intermolecular hydroamination remains limited to a few systems by following the same carbene insertion strategy (*56*, *57*). Instead, intramolecular hydroaminocyclization of a specific class of aniline-tethered alkynes becomes a dominant approach of atroposelective hydroamination (*58*–*61*). Asymmetric hydroamination reactions suffer from limited reaction patterns and chirality patterns. Thus, it is necessary to exploit asymmetric hydroamination by taking advantage of abundant alkynes to fulfill the increasing demand for axially chiral amines. However, intermolecular atroposelective hydroamination remains untraversed, although hydrosilylation and hydrophosphination of sterically demanding alkynes have been accomplished (*62*–*64*).

A pair of enantiomers often exhibit different biological activities, and access to both enantiomers typically requires two catalysts with opposite chirality. To address this limitation, the concept of enantiodivergence has been developed, which refers to generation of both enantiomers in good optical purity starting from the same substrate under different conditions with the same chiral catalyst (*65*). Early examples concerned Lewis acid–catalyzed addition of carbon nucleophiles to carbonyl compounds (*66*–*71*). Recently, You and co-workers (*72*) disclosed an elegant time-dependent enantiodivergent allylic amination system, which involves two sequential kinetic resolutions that proceed at competing rates. In 2021, Zhang and co-workers (*73*) reported Ir-catalyzed enantiodivergent hydrogenation of quinolines, where both enantiomeric products could be obtained in good enantioselectivities in different solvents. Very recently, the Zhang group (*74*) achieved Ti-catalyzed formal enantiodivergent synthesis of chiral alcohols, with the divergence ascribed to the nuclearity of the chiral catalyst. In the regime of C─H bond activation, Li and co-workers (*75*, *76*) reported Cp^XRh(III)-catalyzed enantiodivergent syntheses of chiral heterocycles by subtle adjustment of the achiral carboxylic acid and the reaction solvent. Enantiodivergence has also been realized by subtle changes in the solvent in other metal-catalyzed reactions (*77*, *78*).These outcomes underscored the promise of chiral rhodium(III) catalysts in enantiodivergent catalysis. However, enantiodivergent hydroamination reactions have not been disclosed. The rarity of enantiodivergent synthesis is largely ascribed to challenging control of the enantiodetermining step (EDS). The origin of

[1]Institute of Chemistry Frontier, School of Chemistry and Chemical Engineering, Shandong University, Qingdao 266237, China. [2]Center of Chemistry for Frontier Technologies, Department of Chemistry, State Key Laboratory of Clean Energy Utilization, Zhejiang University, Hangzhou 310027, China. [3]School of Chemistry and Chemical Engineering, Shaanxi Normal University, Xi'an 710062, China. [4]Beijing National Laboratory for Molecular Sciences, Zhongguancun North, First Street No. 2, Beijing 100190, China. [5]State Key Laboratory of Physical Chemistry of Solid Surfaces, Xiamen University, Xiamen 361005, China.
*Corresponding author. Email: lixw@snnu.edu.cn (X.L.); hxchem@zju.edu.cn (X.H.)

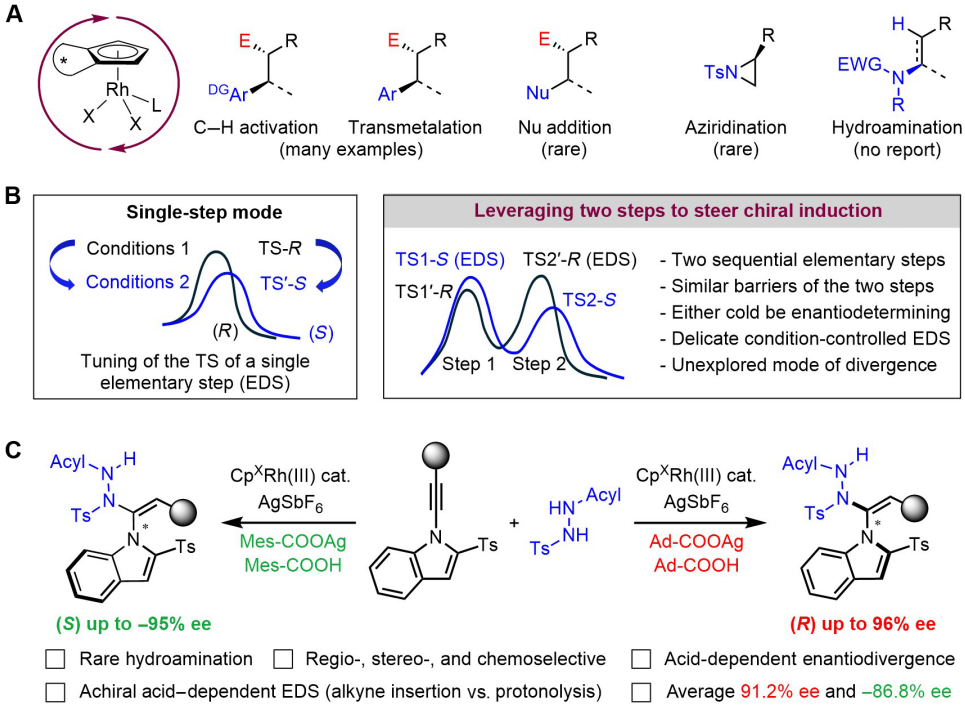

Fig. 1. Rh(III) catalysts in asymmetric catalysis and in enantiodivergent hydroamination. (**A**) Chiral CpXRh(III) catalyst in asymmetric functionalization of unsaturated substrates. (**B**) Modes of enantiodivergent catalysis: Variation of the coordination mode/sphere of the transition state (TS). (**C**) Acid-dependent enantiodivergent alkyne hydroamination: Two-step enantiodetermining mode (this work). Black and blue curves represent different mechanistic details (TSs) of the same elementary step(s), each defining a major enantiomeric product with opposite chirality (only the major enantiomer-forming TS is included for simplicity). EDS, enantiodetermining step; EWG, electron withdrawing group.

divergence is either unclear or predominantly ascribed to tuning of the transition state (TS) of a specific enantiodetermining elementary step such as addition (*71*), C—H activation (*75*), or σ-bond metathesis (Fig. 1B, left) (*76*). Under different conditions, the chirality of the major enantiomeric product is switched by following a TS with an altered coordination number, charge, or coordination sphere. We conceived a working principle by incorporating a second elementary step (Fig. 1B, right). In the case of two sequential elementary steps with comparable barriers in each pathway (black and blue curves), tuning the reaction may result in two consequences. The nature of the TSs may be altered to allow for enantiodivergence (black versus blue). Moreover, the EDS may be switched between the two elementary steps owing to the condition-dependent tuning of the relative barrier and/or thermodynamics of these two steps. This previously unidentified enantiodetermining mode, which intertangles two steps, will leave more room for enantiodivergent control. Nevertheless, this mode has not been investigated because of complicated kinetic and thermodynamic scenarios. We now report our proof-of-concept studies of Rh(III)-catalyzed enantiodivergent hydroamination of sterically hindered alkynes, affording both atropisomeric olefins in high regio-, stereo-, and enantioselectivity (Fig. 1C), where the enantiodivergence was enabled by judicious choice of readily available achiral acids.

RESULTS

Initial optimization studies

Inspired by the reactive Rh(III)—C bonds in diverse asymmetric catalysis, we explored the alternative Rh—N species in asymmetric hydroamination by repurposing the versatile chiral Cp^XRh(III) catalysts. The coupling reaction of an alkyne **1a** and a hydrazine **2a** bearing a chelating group was screened in the presence of $AgSbF_6$ (Table 1). The desired hydroamination reaction proceeded under various conditions in the presence of a Cramer-type rhodium catalyst and a carboxylic acid and its silver salt. The enantioselectivity was found to be significantly affected by the carboxylate. The AcOH/AgOAc participated to give only poor enantioselectivity in all cases (entries 1 to 4). Moving to the PivOH/PivOAg combination improved the enantioselectivity (entry 5), suggesting the superiority of sterically bulky aliphatic acid. The use of $AdCO_2H$/$AdCO_2Ag$ improved the enantioselectivity to 84% enantiomeric excess (ee ;entry 6). The enantioselectivity was further improved to 89% ee when a slightly different (***R***)-**Rh2** catalyst was used in 2,2,2-Trifluoroethanol (TFE) solvent (entry 12), while other catalyst-solvent combinations only gave inferior outcomes (entries 7 to 11). Given the marked effects of the carboxylic acid, a series of benzoic acids was also screened (entries 14 to 18). To our astonishment, the use of a combination of MesCOOH/MesCOOAg afforded product **3** with the opposite and complementary (*S*) configuration in −91% ee, constituting a rare case of enantiodivergent synthesis. In addition, reducing the amount of the acid and its silver salts led to a very sluggish reaction. In the catalytic system, the $AgSbF_6$ additive reacts with the Rh(III) catalyst to pull off the chloride and activates the catalyst, and the RCO_2Ag silver salt works as a suitable weak base to assist in the activation of hydrazine and to promote the reaction conversion. In addition, we also attempted to use (*S*)-2-(1,3-dioxoisoindolin-2-yl)-3,3-dimethylbutanoic acid and its silver salt as the sole chiral source

Table 1. Optimization studies of enantiodivergent hydroamination of an alkyne. Reaction conditions: Reactions were carried out using alkyne **1a** (0.05 mmol), **2a** (1.2 equiv), chiral Rh(III) catalyst (4 mol %), silver carboxylate (2 equiv), and carboxylic acid (2 equiv) at 0°C in a solvent (1 ml) for 12 hours under N_2. Bold font is used to emphasize the reaction standard condition, corresponding to the conditions in Fig. 2. DCM, dichloromethane; HFIP, hexafluoroisopropanol.

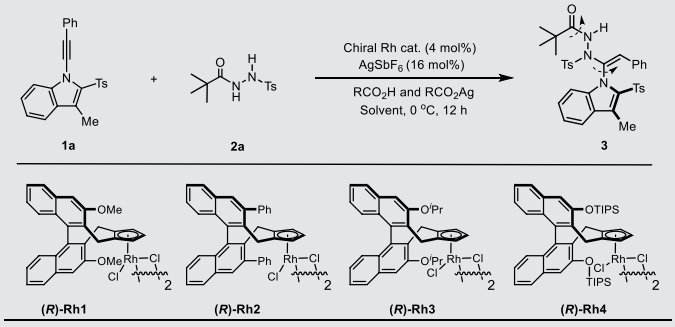

Entry	Rh cat.	R (acid)	Solvent	Yield (%)*	ee (%)†
1	**Rh1**	Me	DCE	47	8
2	**Rh2**	Me	DCE	50	5
3	**Rh3**	Me	DCE	23	7
4	**Rh4**	Me	DCE	<5	–
5	**Rh1**	^{t}Bu	DCE	58	70
6	**Rh1**	**Ad**	**DCE**	**58**	**84**
7	**Rh1**	Ad	DCM	46	76
8	**Rh1**	Ad	$CHCl_3$	40	75
9	**Rh1**	Ad	PhCl	28	70
10	**Rh1**	Ad	TFE	66	81
11	**Rh1**	Ad	HFIP	48	66
12	**Rh2**	**Ad**	**TFE**	**74**	**89**
13‡	**Rh2**	Ad	TFE	48	90
14	**Rh1**	Ph	DCE	54	30
15	**Rh1**	**Mes**	**DCE**	**62**	**−91**
16‡	**Rh1**	Mes	DCE	47	−91
17	**Rh1**	Mes	DCM	60	−90
18	**Rh1**	Mes	$CHCl_3$	55	−86

*Isolated yields. †The ee was determined by high-performance liquid chromatography analysis. ‡At −20°C.

with $[RhCp^*Cl_2]_2$ or $[Ru(p\text{-cymene})Cl_2]_2$ being the catalyst, but no enantioselectivity was detected in either case.

The reaction scope

We next explored the generality of the coupling system under the complementary sets of standard conditions (Fig. 2). The AdCOOH/AdCOOAg (TFE solvent) conditions (condition A) proved generally applicable. The coupling of isobutyryl-functionalized hydrazide proceeded smoothly with indolyl-alkynes bearing different substituents at the three, four, and five positions (**4** to **12**) in excellent enantioselectivity (89 to 95% ee). Variations of the alkyne terminus verified the tolerance of alkyl, aryl, halo, ester, OCF_3, and CF_3 groups at different positions of the benzene ring (**13** to **27**, 87 to 96% ee). The absolute configuration of product **14** has been established as (*R*) by electronic circular dichroism (ECD) spectroscopy and x-ray crystallography (CCDC 2343135; see the Supplementary Materials). The alkyne terminus was also extended to a thienyl group (**28**). Besides the aryl alkyne substrates, several alkyl alkynes were also viable (**29** and **30**), albeit with lower enantioselectivity for **30**. The scope of the hydroaminating reagent was next examined, and primary (**28**), secondary (**33**), and tertiary (**34** to **36**) groups in the hydrazide were compatible, affording the products in generally excellent enantio- or diastereoselectivity (82 to 94% ee). Besides, the sulfonyl group in the hydrazide was extendable to several arenesulfonyls (**37** to **42**, 88 to 94% ee). The synthesis of the (*S*) product was then examined under the complementary MesCOOH/MesCOOAg conditions [(***R***)-**Rh1** catalyst, condition B] for all the substrates. Most of them proceeded in good to excellent enantioselectivities although they tend to be slightly lower than those of the (*R*) configured products obtained under condition A. To our delight, positive exceptions were found for products **27** and **30** to **32**, which were isolated in 92 to 94% ee and in acceptable yields. For the purpose of direct comparisons with the (*S*) configured products under the same catalyst and solvent conditions, the synthesis of the (*R*) configured products was also conducted under condition A′ [(***R***)-**Rh1** catalyst, 1,2-Dichloroethane (DCE)] for selected substrates (products **3**, **6**, **13**, **17** to **21**, **24**, and **39**). In general, good to excellent

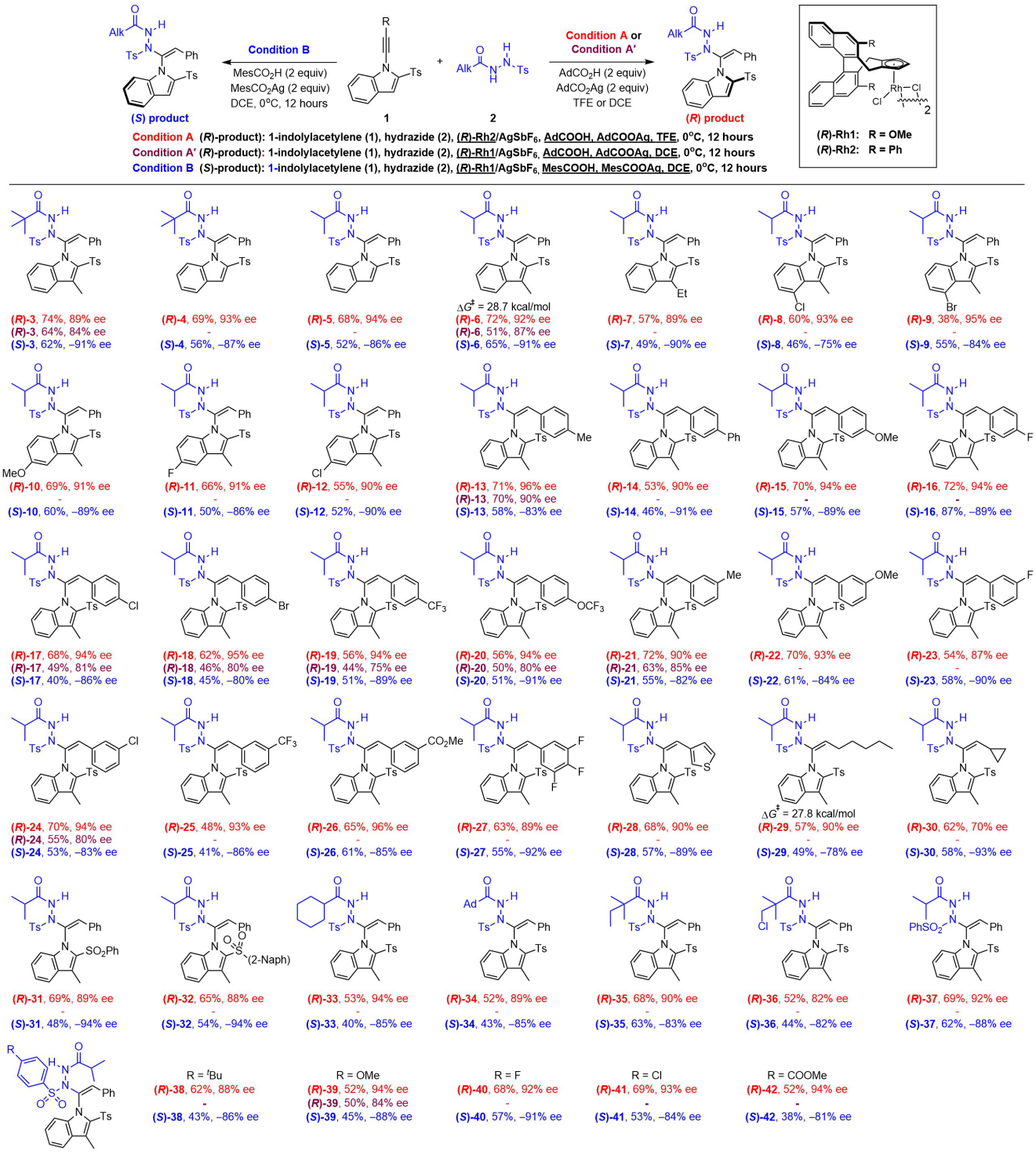

Fig. 2. Scope of the enantiodivergent alkyne hydroamination. Reactions were carried out using alkyne **1** (0.1 mmol), hydrazide **2** (1.2 equiv), **(*R*)-Rh2** (4 mol %), $AgSbF_6$ (16 mol %), and $AdCO_2Ag$/$AdCO_2H$ (2.0 equiv) at 0°C in CF_3CH_2OH (1 ml) for 12 hours under N_2, isolated yields. Reaction condition A′: Reactions were carried out using alkyne **1** (0.1 mmol), hydrazide **2** (1.2 equiv), **(*R*)-Rh1** (4 mol %), $AgSbF_6$ (16 mol %), $AdCO_2Ag$ (2.0 equiv), and $AdCO_2H$ (2.0 equiv) at 0°C in DCE (1 ml) for 12 hours under N_2, isolated yields. Reaction condition B: Reactions were carried out using alkyne **1** (0.1 mmol), hydrazide **2** (1.2 equiv), **(*R*)-Rh1** (4 mol %), $AgSbF_6$ (16 mol %), $MesCO_2Ag$ (2.0 equiv), and $MesCO_2H$ (2.0 equiv) at 0°C in DCE (1 ml) for 12 hours under N_2, isolated yields. Only selected substrates were examined under condition A′, and those not given refer to reactions not performed.

enantioselectivity (75 to 90% ee, average 82.7% ee) was still obtained, and the trend of enantiodivergence is quite pronounced. The configurational stability has been measured for products **5** (racemization $\Delta G^{\neq} = 28.7$ kcal/mol) and **29** (racemization $\Delta G^{\neq} = 27.8$ kcal/mol). Thus, these products are relatively labile, which accordingly requires rather mild reaction conditions. Notably, while each racemic product was well resolvable into two signals using high-performance liquid chromatography analyses, each product appears as two rotamers in ^{1}H and ^{13}C nuclear magnetic resonance (NMR) spectroscopy, and the fluxionality in the NMR timescale is ascribed to the hindered rotation along both the amide bond (calculated $\Delta G^{\neq} = 21.7$ kcal/mol), as has been confirmed by variable temperature NMR analyses.

Synthetic applications

We next briefly demonstrated the synthetic applications of a product (Fig. 3). Treatment of product **5** with a diazo reagent in the presence of an achiral Rh(II) catalyst afforded the *N*-alkylated product **43** in good yield as a single diastereomer with essentially no erosion of the enantiopurity (Fig. 3A). This transformation introduced a new N—N chiral axis upon dynamic kinetic transformation of the N—H bond through chiral induction. As expected, signals with normal linewidths were detected in the NMR spectra of **43**. The reaction of (*rac*)-**4** and CH_3I, KOH in MeOH led to the conversion of the N-Ts group to N-OMe (**44**) (Fig. 3B). As a special amide, product **5** was applied as a chiral additive in Ru-catalyzed annulative coupling of a sulfoximine with a sulfoxonium ylide reagent, affording product **45** in moderate enantioselectivity (Fig. 3C).

Experimental mechanistic studies

Experimental studies have been conducted to explore the mechanism (Fig. 4). The stoichiometric reaction of hydrazide **2b** and (***R***)-**Rh1** or (***R***)-**Rh2** in the presence of a base afforded cyclometalated complex **46** or **47**, respectively, as a single diastereomer (Fig. 4A), and complex **47** has been characterized by x-ray crystallography (CCDC2343134). Application of the complex **46** as a catalyst under otherwise the same conditions afforded the chiral product with comparable enantioselectivity under each set of conditions (Fig. 4B). In contrast, omission of the $AgSbF_6$ additive completely inhibited the reaction, suggesting the intermediacy of a cationic Rh(III) species. To explore the role of carboxylic acid/silver carboxylate, parallel kinetic isotope effect (KIE) experiments have been conducted using protio and deterio carboxylic acids under the two sets of reaction conditions (Fig. 4C). A small KIE (= 1.4) was obtained under the (*R*)-enriched condition A′ using $AdCO_2H/AdCO_2D$. However, a larger KIE = 2.8 was detected under condition B. The latter KIE value suggests that the protonolysis that forms the C—H/D bond is probably involved in the turnover-limiting step, while the former small value may indicate that the barrier of protonolysis only contributes insignificantly to the overall kinetic barrier (vide infra). In addition, equimolar mixtures of AdCOOH/AdCOOAg/MesCOOH/MesCOOAg were applied as additives to the coupling of **1** and **2b**, and product **6** was (*S*)-enriched with −40% ee (Fig. 4D), suggesting that the MesCOOH/Ag overrode the AdCOOH/Ag in terms of the activity (vide infra).

Computational mechanistic studies

The origin of the enantiodivergence of the coupling of alkyne **1** and hydrazide **2b** was next elucidated (giving **6**) by computational studies at the M06/def2-TZVP-SMD(DCE)//B3LYP-D3(BJ)/def2-SVP level of theory (Fig. 5). Starting for a cationic species as suggested by our experimental studies, the subsequent alkyne insertion and protonolysis have been interrogated in the same solvent (DCE) using different acids. The AdCOOH conditions were explored first (Fig.

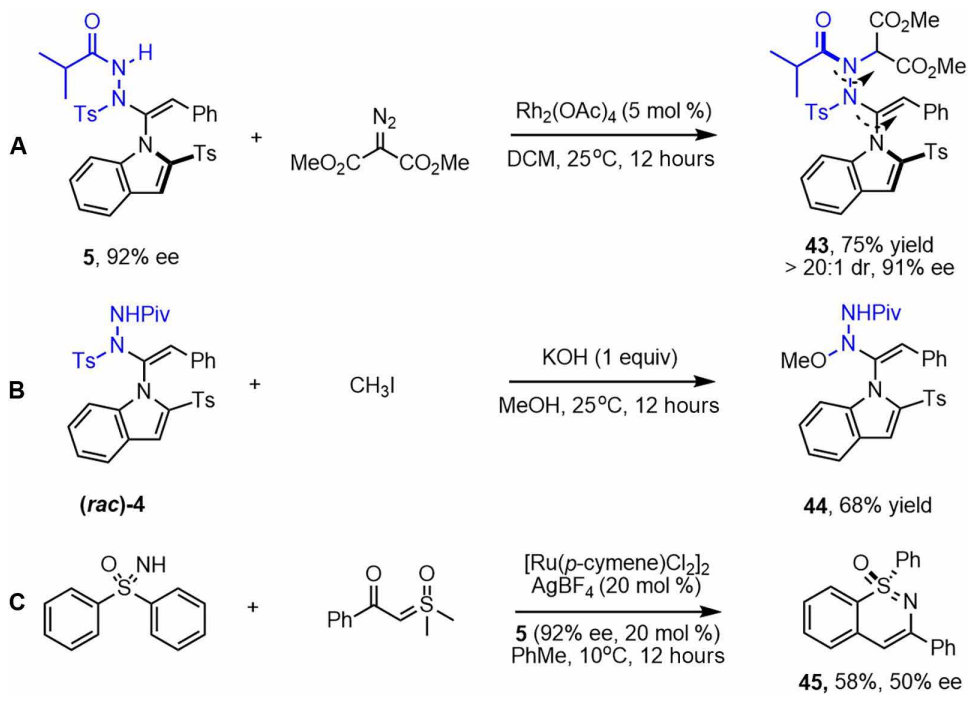

Fig. 3. Synthetic applications of representative products. (A) N—H alkylation of product 5. **(B)** The conversion of N-Ts group to N-OMe. **(C)** Product 5 as a chiral additive in Ru-catalyzed annulative coupling.

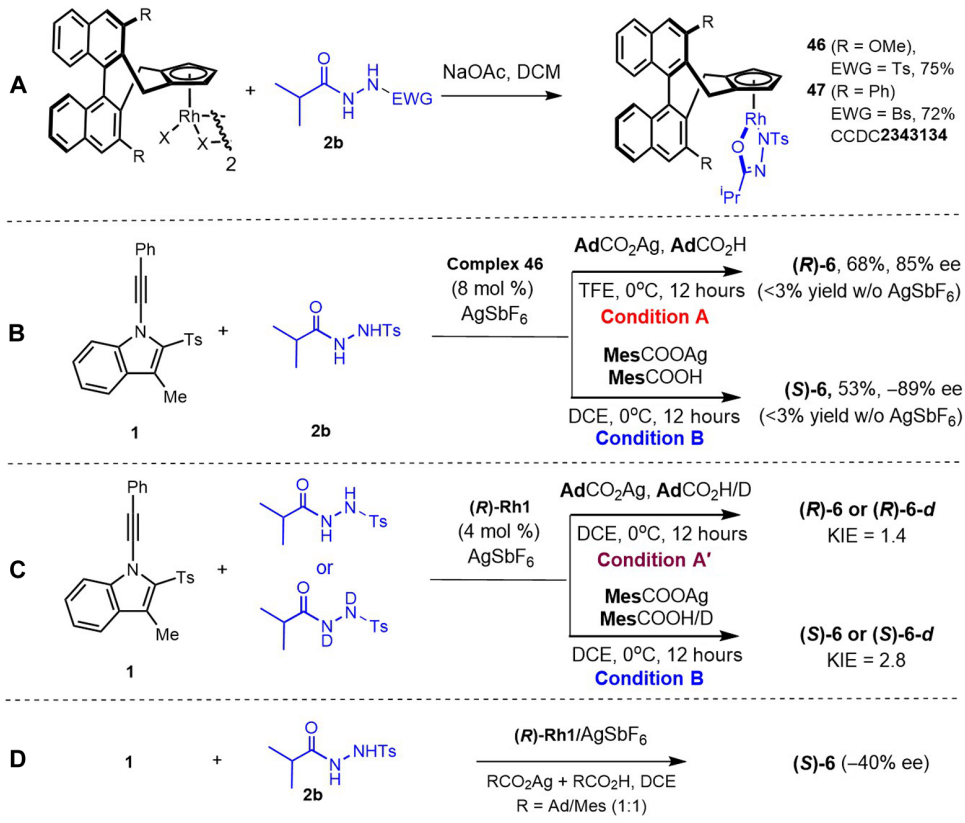

Fig. 4. Experimental mechanistic studies. (A) Intermediate separation. **(B)** Intermediate studies. **(C)** KIE studies. **(D)** Competition experiment.

5A). The alkyne may approach from the left or the right side of the rhodium toward insertion, and this insertion is likely independent of the carboxylic acid. Meanwhile, the Ts group in the indole may be pointed frontward or backward. These combinations resulted in four possible mechanistic scenarios defined by four diastereomeric intermediates based on the rhodium central chirality and the axial chirality. Of these four intermediates, two eventually lead to the (*R*)-**6** product (Fig. 5A, left), and the other two lead to the (*S*)-**6** product (Fig. 5A, right). The lowest barrier (11.6 kcal/mol) of alkyne insertion was found to proceed through the **TS2** as a result of intraligand π-π interactions (see the Supplementary Materials). However, the subsequent protonolysis by $AdCO_2H$ proceeds with a relatively high energy barrier of 21.9 kcal/mol (**TS10**). In contrast, the insertion of alkyne **1a** with an opposite trajectory via the **TS5** bears a barrier of 15.7 kcal/mol, and the subsequent protonolysis occurs with a lower TS (**TS13**, 13.2 kcal/mol, yellow line and labels), which constitutes the lowest energy pathway, with the alkyne insertion being rate and enantiodetermining. The competing pathway was found to occur via the **TS3** (17.2 kcal/mol) and **TS11** (red labels), which corresponds to a $\Delta\Delta G^{\neq} = 1.5$ kcal/mol, favoring the (*R*) product. The calculated data are in line with our experimentally observed 87% ee of product (*R*)-**6** under the condition A′. In addition, the small KIE of 1.4 is also consistent with the computational results because the protonolysis occurs after the rate-limiting step.

In the case of the $MesCO_2H$ (Fig. 5B), the lowest insertion pathway coincides with the lowest overall energy pathway (13.6 kcal/mol) with the protonolysis being enantio- and rate determining via **TS14** (green lines), favoring the formation of the (*S*)-**6** product with a significantly lower energy of the **TS14** compared with that using AdCOOH as an acid. The second lowest energy competing pathway was found to occur via the **TS5** and **TS17** with an overall barrier of 15.7 kcal/mol (red labels), which corresponds to a $\Delta\Delta G^{\neq} = 2.1$ kcal/mol, favoring the (*S*) product. This result is well consistent with the observed 91% ee of (*S*)-**6** under the condition B. Our observed KIE = 2.8 is in line with the calculated lowest energy pathway where protonolysis is rate limiting. The overriding activity of MesCOOH/Ag over the AdCOOH/Ag in competition reactions (Fig. 4D) is also qualitatively consistent with the lower calculated overall barrier for the former acid (13.6 versus 15.7 kcal/mol).

DISCUSSION

Our DFT data verified that, in the protonolysis of a given rhodium-alkenyl species, a stronger carboxylic acid (MesCOOH) tends to give a lower barrier (Fig. 5). Experimentally, our screening studies using different acids/silver salts revealed that aliphatic carboxylic acids and relatively weak aromatic carboxylic acids tend to produce the (*R*) product (see the Supplementary Materials). Only when the acidity of the aromatic acid is sufficiently high [calculated $pK_a < 2.4$ (where *K*a is the acid dissociation constant)] was the (*S*) product started to be observed as the major enantiomer. These experimental and DFT data collectively revealed that the acid plays a role in affecting the barrier of the protonolysis since it is not relevant during the alkyne insertion. This barrier and the barrier of alkyne insertion collectively determine the enantioselectivity of this system. Thus, the enantiodivergence originates from a switch of the EDS as dictated by the acid additive.

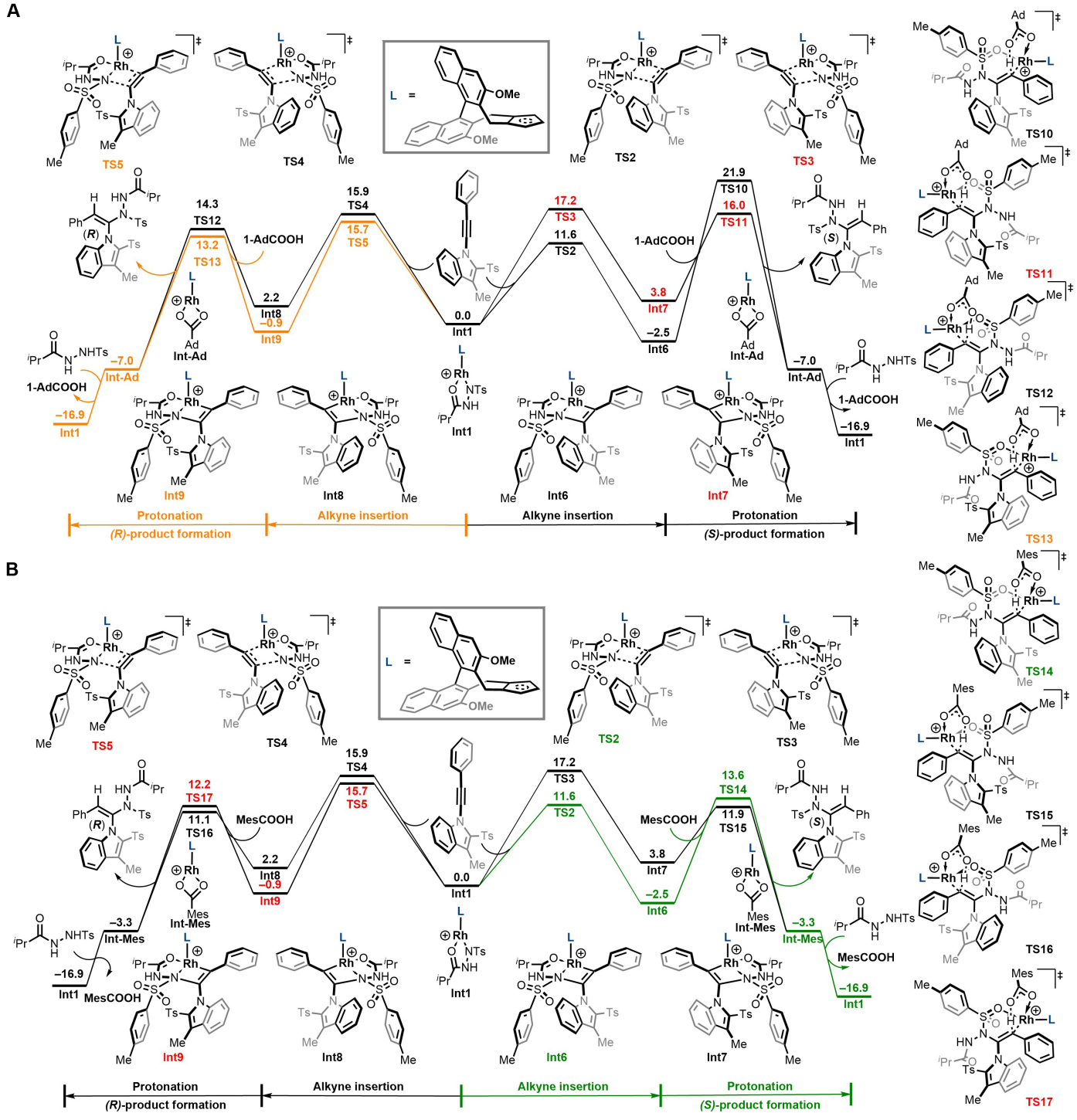

Fig. 5. Potential energy surface of the alkyne insertion and protonolysis using different acids in DCE solvent. (**A**) Free energy profile of the alkyne insertion-protonolysis using AdCOOH (DCE solvent). (**B**) Free energy profile of the alkyne insertion-protonolysis using MesCOOH (DCE solvent).

In the case of a relatively strong acid (MesCOOH), the protonation barrier generally decreases compared to that by using AdCOOH (Fig. 5, A, right, versus B, right). The reaction can then proceed with the lowest barrier via the protonolysis of **Int6** that is defined by the lowest generation barrier via the **TS2**, with the protonolysis being rate limiting. In contrast, in the case of AdCOOH, changes in the axial chirality of the diastereomeric **Int9** (and **TS13**) lead to the change of the orientation of the Ts group, which corresponds to a decrease in repulsions (between the Ph and the chiral ligand) and a lower energy barrier in protonolysis to give the (*R*) isomer with alkyne insertion being enantiodetermining. We also attempted but failed to isolate the intermediate **Int6** under various stoichiometric

conditions, and only unidentifiable metal species was detected together with a small amount of the final organic product, likely due to the low overall barrier of this catalytic system. Nevertheless, our computational and experimental studies consistently supported the proposed mechanism in this system. Thus, our system constitutes a rare example of enantiodivergence via leveraging two potential EDSs with two slightly different overall kinetic barriers.

In summary, we have repurposed the well-studied chiral $Cp^XRh(III)$ catalyst as a catalyst toward the first intermolecular atroposelective hydroamination of alkynes. The coupling system proceeded with excellent regio-, stereo-, and enantioselectivity. Enantiodivergence has been realized under acid control. When catalyzed by the same or closely analogous chiral Rh(III) catalyst, the use of AdCOOH delivered the (*R*) product, while the presence of MesCOOH afforded the (*S*) isomer as the major product. Mechanistic studies revealed that the enantiodivergence originates from the switch of the EDS (alkyne insertion versus protonolysis) under acid control, which constitutes a working mode of enantiodivergence by leveraging two elementary steps. This working model is expected to offer insight into the development of other enantiodivergent systems.

MATERIALS AND METHODS

Synthesis of 3 to 42

Reaction condition A

A screw-cap vial (8 ml) was charged with indolyl-alkyne (0.12 mmol, 1.2 equiv), sulfonyl hydrazine 2 (0.1 mmol, 1.0 equiv), **(*R*)-Rh2** (5.4 mg, 4 mol %), $AgSbF_6$ (5.5 mg, 16 mol %), AdCOOAg (57.4 mg, 0.2 mmol, 2.0 equiv), AdCOOH (36.0 mg, 0.2 mmol, 2.0 equiv), and TFE (1 ml). The reaction mixture was vigorously stirred at 0°C for 12 hours under N_2. The reaction mixture was evaporated under vacuum, and the residue was purified by preparative thin-layer chromatography (TLC) to give the corresponding (*R*)-enriched product.

Reaction condition A′

A screw-cap vial (8 ml) was charged with indolyl-alkyne (0.12 mmol, 1.2 equiv), sulfonyl hydrazine **2** (0.1 mmol, 1.0 equiv), **(*R*)-Rh1** (4.6 mg, 4 mol %), $AgSbF_6$ (5.5 mg, 16 mol %), AdCOOAg (57.4 mg, 0.2 mmol, 2.0 equiv), AdCOOH (36.0 mg, 0.2 mmol, 2.0 equiv), and DCE (1 ml). The reaction mixture was vigorously stirred at 0°C for 12 hours under N_2. The reaction mixture was evaporated under vacuum, and the residue was purified by preparative TLC to give the corresponding (*R*)-enriched product.

Reaction condition B

A screw-cap vial (8 ml) was charged with indolyl-alkyne (0.12 mmol, 1.2 equiv), sulfonyl hydrazine **2** (0.1 mmol, 1.0 equiv), **(*R*)-Rh1** (4.6 mg, 4 mol %), $AgSbF_6$ (5.5 mg, 16 mol %), MesCOOAg (54.4 mg, 0.2 mmol, 2.0 equiv), MesCOOH (32.8 mg, 0.2 mmol, 2.0 equiv), and DCE (1 ml). The reaction mixture was vigorously stirred at 0°C for 12 hours under N_2. The reaction mixture was evaporated under vacuum, and the residue was purified by preparative TLC to give the corresponding (*S*)-enriched product.

Supplementary Materials

This PDF file includes:

Supplementary Text
Figs. S1 to S4
Tables S1 to S4
References

REFERENCES AND NOTES

1. B. Ye, N. Cramer, Chiral cyclopentadienyls: Enabling ligands for asymmetric Rh(III)-catalyzed C–H functionalizations. *Acc. Chem. Res.* **48**, 1308–1318 (2015).
2. C. G. Newton, D. Kossler, N. Cramer, Asymmetric catalysis powered by chiral cyclopentadienyl ligands. *J. Am. Chem. Soc.* **138**, 3935–3941 (2016).
3. C. G. Newton, S.-G. Wang, C. C. Oliveira, N. Cramer, Catalytic enantioselective transformations involving C–H bond cleavage by transition-metal complexes. *Chem. Rev.* **117**, 8908–8976 (2017).
4. T. Yoshino, S. Satake, S. Matsunaga, Diverse approaches for enantioselective C–H functionalization reactions using group 9 Cp^xM^{III} catalysts. *Chem. A Eur. J.* **26**, 7346–7357 (2020).
5. Q. Shao, K. Wu, Z. Zhuang, S. Qian, J.-Q. Yu, From $Pd(OAc)_2$ to chiral catalysts: The discovery and development of bifunctional mono-N-protected amino acid ligands for diverse C–H functionalization reactions. *Acc. Chem. Res.* **53**, 833–851 (2020).
6. Ł. Woźniak, J.-F. Tan, Q.-H. Nguyen, A. M. Vigné, V. Smal, Y.-X. Cao, N. Cramer, Catalytic enantioselective functionalizations of C–H bonds by chiral iridium complexes. *Chem. Rev.* **120**, 10516–10543 (2020).
7. J. Mas-Roselló, A. G. Herraiz, B. Audic, A. Laverny, N. Cramer, Chiral cyclopentadienyl ligands: Design, syntheses, and applications in asymmetric catalysis. *Angew. Chem. Int. Ed. Engl.* **60**, 13198–13224 (2021).
8. C. Davies, S. Shaaban, H. Waldmann, Asymmetric catalysis with chiral cyclopentadienyl complexes to access privileged scaffolds. *Trends Chem.* **4**, 318–330 (2022).
9. Q. Zhang, L.-S. Wu, B.-F. Shi, Forging C–heteroatom bonds by transition-metal-catalyzed enantioselective C–H functionalization. *Chem* **8**, 384–413 (2022).
10. H. Yang, B.-B. Gou, H.-T. Dai, Q. Gu, S.-L. You, Advances in the synthesis of chiral cyclopentadienyl ligands and metal complexes. *Sci. Sin. Chim.* **53**, 359–374 (2023).
11. T. K. Achar, S. A. Al-Thabaiti, M. Mokhtar, D. Maiti, Enantioselective annulation reactions through $C(sp^2)$–H activation with chiral Cp^xM^{III} catalysts. *Chem Catal.* **3**, 100575 (2023).
12. C.-X. Liu, S.-Y. Yin, F. Zhao, H. Yang, Z. Feng, Q. Gu, S.-L. You, Rhodium-catalyzed asymmetric C–H functionalization reactions. *Chem. Rev.* **123**, 10079–10134 (2023).
13. S. Choppin, J. Wencel-Delord, Sulfoxide-directed or 3D-metal catalyzed C–H activation and hypervalent iodines as tools for atroposelective synthesis. *Acc. Chem. Res.* **56**, 189–202 (2023).
14. X. Yan, J. Jiang, J. Wang, A class of readily tunable planar-chiral cyclopentadienyl rhodium(III) catalysts for asymmetric C–H activation. *Angew. Chem. Int. Ed. Engl.* **61**, e202201522 (2020).
15. G. Li, X. Yan, J. Jiang, H. Liang, C. Zhou, J. Wang, Chiral bicyclo[2.2.2]octane-fused CpRh complexes: Synthesis and potential use in asymmetric C–H activation. *Angew. Chem. Int. Ed. Engl.* **59**, 22436–22440 (2020).
16. J. Zheng, W. J. Cui, C. Zheng, S.-L. You, Synthesis and application of chiral spiro Cp ligands in rhodium-catalyzed asymmetric oxidative coupling of biaryl compounds with alkenes. *J. Am. Chem. Soc.* **138**, 5242–5245 (2016).
17. W.-J. Cui, Z.-J. Wu, Q. Gu, S.-L. You, Divergent synthesis of tunable cyclopentadienyl ligands and their application in Rh-catalyzed enantioselective synthesis of isoindolinone. *J. Am. Chem. Soc.* **142**, 7379–7385 (2020).
18. B. Ye, N. Cramer, A tunable class of chiral Cp ligands for enantioselective rhodium(III)-catalyzed C–H allylations of benzamides. *J. Am. Chem. Soc.* **135**, 636–639 (2013).
19. B. Ye, N. Cramer, Chiral cyclopentadienyl ligands as ttereocontrolling element in asymmetric C–H functionalization. *Science* **338**, 504–506 (2012).
20. T. K. Hyster, L. Knörr, T. R. Ward, T. Rovis, Biotinylated Rh(III) complexes in engineered streptavid in for accelerated asymmetric C–H activation. *Science* **338**, 500–503 (2012).
21. Z.-J. Jia, C. Merten, R. Gontla, C. G. Daniliuc, A. P. Antonchick, H. Waldmann, General enantioselective C–H activation with efficiently tunable cyclopentadienyl ligands. *Angew. Chem. Int. Ed. Engl.* **56**, 2429–2434 (2012).
22. Ł. Woźniak, N. Cramer, Atropo-enantioselective oxidation-enabled iridium(III)-catalyzed C–H arylations with aryl boronic esters. *Angew. Chem. Int. Ed. Engl.* **60**, 18532–18536 (2021).
23. P. Hu, B. Liu, F. Wang, R. Mi, X.-X. Li, X. Li, A stereodivergent–convergent chiral induction mode in atroposelective access to biaryls via rhodium-catalyzed C–H bond activation. *ACS Catal.* **12**, 13884–13896 (2022).
24. J. Wang, X. Li, Rhodium-catalyzed enantio- and diastereoselective carboamidation of bicyclic olefins toward construction of remote chiral centers and axis. *Sci. China Chem.* **66**, 2046–2052 (2023).
25. M. Tian, D. Bai, G. Zheng, J. Chang, X. Li, Rh(III)-catalyzed asymmetric synthesis of axially chiral biindolyls by merging C–H activation and nucleophilic cyclization. *J. Am. Chem. Soc.* **141**, 9527–9532 (2019).
26. A. J. Zoll, J. C. Molas, B. Q. Mercado, J. A. Ellman, Imine directed Cp*RhIII-catalyzed N–H functionalization and annulation with amino amides, aldehydes, and diazo compounds. *Angew. Chem. Int. Ed. Engl.* **62**, e202210822 (2023).

27. S. Bera, S. Roy, S. C. Pal, A. Anoop, R. Samanta, Iridium(III)-catalyzed intermolecular mild N-arylation of aliphatic amides using quinoid carbene: A migratory insertion based approach. *ACS Catal.* **11**, 10847–10854 (2021).
28. X. Li, H. Song, S. Yu, R. Mi, X.-X. Li, Rhodium-catalyzed enantioselective 1,4-oxyamination of conjugated *gem*-difluorodienes via coupling with carboxylic acids and dioxazolones. *Angew. Chem. Int. Ed. Engl.* **62**, e202305669 (2023).
29. P. Gross, H. Im, D. Laws III, B. Park, M.-H. Baik, S. B. Blakey, Enantioselective aziridination of unactivated terminal alkenes using a planar chiral Rh(III) indenyl catalyst. *J. Am. Chem. Soc.* **146**, 1447–1454 (2024).
30. J. Wang, M.-P. Luo, Y.-J. Gu, Y.-Y. Liu, Q. Yin, S.-G. Wang, Chiral Cp^xrhodium(III)-catalyzed enantioselective aziridination of unactivated terminal alkenes. *Angew. Chem. Int. Ed. Engl.* **63**, e202400502 (2024).
31. F. Pohlki, S. Doye, The catalytic hydroamination of alkynes. *Chem. Soc. Rev.* **32**, 104–114 (2003).
32. S. Hong, T. J. Marks, Organolanthanide-catalyzed hydroamination. *Acc. Chem. Res.* **37**, 673–686 (2004).
33. K. C. Hultzsch, Transition metal-catalyzed asymmetric hydroamination of alkenes (AHA). *Adv. Synth. Catal.* **347**, 367–391 (2005).
34. P. Koschker, B. Breit, Branching out: Rhodium-catalyzed allylation with alkynes and allenes. *Acc. Chem. Res.* **49**, 1524–1536 (2016).
35. J. Escorihuela, A. Lledós, G. Ujaque, Anti-Markovnikov intermolecular hydroamination of alkenes and alkynes: A mechanistic view. *Chem. Rev.* **123**, 9139–9203 (2023).
36. S. Ma, J. F. Hartwig, Progression of hydroamination catalyzed by late transition-metal complexes from activated to unactivated alkenes. *Acc. Chem. Res.* **56**, 1565–1577 (2023).
37. H.-L. Teng, Y. Luo, B. Wang, L. Zhang, M. Nishiura, Z. Hou, Synthesis of chiral amino cyclopropanes by rare-earth-metal-catalyzed cyclopropene hydroamination. *Angew. Chem. Int. Ed. Engl.* **55**, 15406–15410 (2016).
38. K. Xu, Y.-H. Wang, V. Khakyzadeh, B. Breit, Asymmetric synthesis of allylic amines via hydroamination of allenes with benzophenone imine. *Chem. Sci.* **7**, 3313–3316 (2016).
39. H.-L. Teng, Y. Luo, M. Nishiura, Z. Hou, Diastereodivergent asymmetric carboamination/annulation of cyclopropenes with amino alkenes by chiral lanthanum catalysts. *J. Am. Chem. Soc.* **139**, 16506–16509 (2017).
40. S. Park, S. J. Malcolmson, Development and mechanistic investigations of enantioselective Pd-catalyzed intermolecular hydroaminations of internal dienes. *ACS Catal.* **8**, 8468–8476 (2018).
41. L. J. Hilpert, S. V. Sieger, A. M. Haydl, B. Breit, Palladium-and rhodium-catalyzed dynamic kinetic resolution of racemic internal allenes towards chiral pyrazoles. *Angew. Chem. Int. Ed. Engl.* **58**, 3378–3381 (2019).
42. A. Y. Jiu, H. S. Slocumb, C. S. Yeung, X.-H. Yang, V. M. Dong, Enantioselective addition of pyrazoles to dienes. *Angew. Chem. Int. Ed. Engl.* **60**, 19660–19664 (2021).
43. Y. Xi, S. Ma, J. F. Hartwig, Catalytic asymmetric addition of an amine N–H bond across internal alkenes. *Nature* **588**, 254–260 (2020).
44. M. Wang, J. C. Simon, M. Xu, S. A. Corio, J. S. Hirschi, V. M. Dong, Copper-catalyzed hydroamination: Enantioselective addition of pyrazoles to cyclopropenes. *J. Am. Chem. Soc.* **145**, 14573–14580 (2023).
45. C. J. Moody, Enantioselective insertion of metal carbenes into N–H bonds: A potentially versatile route to chiral amine derivatives. *Angew. Chem. Int. Ed. Engl.* **46**, 9148–9150 (2007).
46. B. Liu, S.-F. Zhu, W. Zhang, C. Chen, Q.-L. Zhou, Highly enantioselective insertion of carbenoids into N-H bonds catalyzed by copper complexes of chiral spiro bisoxazolines. *J. Am. Chem. Soc.* **129**, 5834–5835 (2007).
47. E. C. Lee, G. C. Fu, Copper-catalyzed asymmetric N-H insertion reactions: Couplings of diazo compounds with carbamates to generate α-amino acids. *J. Am. Chem. Soc.* **129**, 12066–12067 (2007).
48. B. Xu, S.-F. Zhu, X.-L. Xie, J.-J. Shen, Q.-L. Zhou, Asymmetric N–H insertion reaction cooperatively catalyzed by rhodium and chiral spiro phosphoric acids. *Angew. Chem. Int. Ed. Engl.* **50**, 11483–11486 (2011).
49. X. Xu, P. Y. Zavalij, M. P. Doyle, Synthesis of tetrahydropyridazines by a metal–carbene-directed enantioselective vinylogous N-H insertion/lewis acid-catalyzed diastereoselective Mannich addition. *Angew. Chem. Int. Ed. Engl.* **51**, 9829–9833 (2012).
50. S.-F. Zhu, B. Xu, G.-P. Wang, Q.-L. Zhou, Well-defined binuclear chiral spiro copper catalysts for enantioselective N–H insertion. *J. Am. Chem. Soc.* **134**, 436–442 (2012).
51. V. Arredondo, S. C. Hiew, E. S. Gutman, I. D. Premachandra, D. L. Van Vranken, Enantioselective palladium-catalyzed carbene insertion into the N–H bonds of aromatic heterocycles. *Angew. Chem. Int. Ed. Engl.* **56**, 4156–4159 (2017).
52. W. Yang, M. Pu, X. Lin, M. Chen, Y. Song, X. Liu, Y.-D. Wu, X. Feng, Enantioselective formal vinylogous N–H insertion of secondary aliphatic amines catalyzed by a high-spin cobalt(II) complex. *J. Am. Chem. Soc.* **143**, 9648–9656 (2021).
53. Y. Li, Y.-X. Su, Y.-T. Zhao, L. Liu, M.-L. Li, S.-F. Zhu, Enantioselective synthesis of unnatural carbamate-protected α-alkyl amino esters via N–H bond insertion reactions. *ACS Catal.* **12**, 13143–13148 (2022).
54. Q. Peng, M. Huang, G. Xu, Y. Zhu, Y. Shao, S. Tang, X. Zhang, J. Sun, Asymmetric N-alkylation of 1H-indoles via carbene insertion reaction. *Angew. Chem. Int. Ed. Engl.* **62**, e202313091 (2023).
55. J.-B. Pan, X.-G. Zhang, Y.-F. Shi, A.-C. Han, Y.-J. Chen, J. Ouyang, M.-L. Li, Q.-L. Zhou, A spiro phosphamide catalyzed enantioselective proton transfer of ylides in a free carbene insertion into N–H bonds. *Angew. Chem. Int. Ed. Engl.* **62**, e202300691 (2023).
56. C. Niu, Y. Zhou, Q. Chen, Y. Zhu, S. Tang, Z.-X. Yu, J. Sun, Atroposelective synthesis of N-arylindoles via enantioselective N–H bond insertion. *Org. Lett.* **24**, 7428–7433 (2022).
57. Q. Ren, M. Lang, H. Liu, X. Li, D. Wu, J. Wu, M. Yang, J. Wei, Z. Ren, L. Wang, Stereocontrol of C–N axial and spiro-central chirality via Rh(II)-catalyzed enantioselective N–H bond insertion of indolinone-spiroacetal. *Org. Lett.* **25**, 7745–7750 (2023).
58. N. Ototake, Y. Morimoto, A. Mokuya, H. Fukaya, Y. Shida, O. Kitagawa, Catalytic enantioselective synthesis of atropisomeric indoles with an N-C chiral axis. *Chem. A Eur. J.* **16**, 6752–6755 (2010).
59. L. Peng, K. Li, C. Xie, S. Li, D. Xu, W. Qin, H. Yan, Organocatalytic asymmetric annulation of ortho-alkynylanilines: Synthesis of axially chiral naphthyl-C2-indoles. *Angew. Chem. Int. Ed. Engl.* **58**, 17199–17204 (2019).
60. Z.-S. Wang, L.-J. Zhu, C.-T. Li, B.-Y. Liu, X. Hong, L.-W. Ye, Synthesis of axially chiral N-arylindoles via atroposelective cyclization of ynamides catalyzed by chiral Brønsted acids. *Angew. Chem. Int. Ed. Engl.* **61**, e202201436 (2022).
61. C.-S. Wang, Q. Xiong, H. Xu, H.-R. Yang, Y. Dang, X.-Q. Dong, C.-J. Wang, Organocatalytic atroposelective synthesis of axially chiral *N*, *N*′-pyrrolylindoles via de novo indole formation. *Chem. Sci.* **14**, 12091–12097 (2023).
62. D. Ji, J. Jing, Y. Wang, Z. Qi, F. Wang, X. Zhang, Y. Wang, X. Li, Palladium-catalyzed asymmetric hydrophosphination of internal alkynes: Atroposelective access to phosphine-functionalized olefins. *Chem* **8**, 3346–3362 (2022).
63. B. Cai, Y. Cui, J. Zhou, Y.-B. Wang, L. Yang, B. Tan, J. Wang, Asymmetric hydrophosphinylation of alkynes: Facile access to axially chiral styrene-phosphines. *Angew. Chem. Int. Ed. Engl.* **62**, e202215820 (2023).
64. Q. Wu, Q. Zhang, S. Yin, A. Lin, S. Gao, H. Yao, Atroposelective synthesis of axially chiral styrenes by platinum-catalyzed stereoselective hydrosilylation of internal alkynes. *Angew. Chem. Int. Ed. Engl.* **62**, e202305518 (2023).
65. I. P. Beletskaya, C. Nájera, M. Yus, Stereodivergent catalysis. *Chem. Rev.* **118**, 5080–5200 (2018).
66. D. A. Evans, C. S. Burgey, M. C. Kozlowski, S. W. Tregay, C_2-symmetric copper (II) complexes as chiral lewis acids. Scope and mechanism of the catalytic enantioselective aldol additions of enolsilanes to pyruvate esters. *J. Am. Chem. Soc.* **121**, 686–699 (1999).
67. B. M. Trost, A. Fettes, B. T. Shireman, Direct catalytic asymmetric aldol additions of methyl ynones. Spontaneous reversal in the sense of enantioinduction. *J. Am. Chem. Soc.* **126**, 2660–2661 (2004).
68. F. Lutz, T. Igarashi, T. Kawasaki, K. Soai, Small amounts of achiral β-amino alcohols reverse the enantioselectivity of chiral catalysts in cooperative asymmetric autocatalysis. *J. Am. Chem. Soc.* **127**, 12206–12207 (2005).
69. Y. Sohtome, S. Tanaka, K. Takada, T. Yamaguchi, K. Nagasawa, Solvent-dependent enantiodivergent Mannich-type reaction: Utilizing a conformationally flexible guanidine/bisthiourea organocatalyst. *Angew. Chem. Int. Ed. Engl.* **49**, 9254–9257 (2010).
70. Y.-C. Chan, X. Wang, Y.-P. Lam, J. Wong, Y.-L. Steve Tse, Y.-Y. Yeung, A catalyst-controlled enantiodivergent bromolactonization. *J. Am. Chem. Soc.* **143**, 12745–12754 (2021).
71. J. Zhou, M.-C. Ye, Z.-Z. Huang, Y. Tang, Controllable enantioselective Friedel-Crafts reaction between indoles and alkylidene malonates catalyzed by pseudo-C_3-symmetric trisoxazoline copper(II) complexes. *J. Org. Chem.* **69**, 1309–1320 (2004).
72. H.-F. Tu, P. Yang, Z.-H. Lin, C. Zheng, S.-L. You, Time-dependent enantiodivergent synthesis via sequential kinetic resolution. *Nat. Chem.* **12**, 838–844 (2020).
73. Z. Han, G. Liu, X. Yang, X.-Q. Dong, X. Zhang, Enantiodivergent synthesis of chiral tetrahydroquinoline derivatives via Ir-catalyzed asymmetric hydrogenation: Solvent-dependent enantioselective control and mechanistic investigations. *ACS Catal.* **11**, 7281–7291 (2021).
74. S. Li, H. Zhu, L. Li, W. Chen, J. Jiang, Z.-W. Qu, S. Grimme, Y.-Q. Zhang, A nuclearity-dependent enantiodivergent epoxide opening via enthalpy-controlled mononuclear and entropy-controlled dinuclear (salen)titanium catalysis. *Angew. Chem. Int. Ed. Engl.* **62**, e202309525 (2023).
75. B. Shen, B. Wan, X. Li, Enantiodivergent desymmetrization in the rhodium(III)-catalyzed annulation of sulfoximines with diazo compounds. *Angew. Chem. Int. Ed. Engl.* **57**, 15534–15538 (2018).
76. P. Wang, H. Wu, X.-P. Zhang, G. Huang, R. H. Crabtree, X. Li, Sigma-bond metathesis as an unusual asymmetric induction step in rhodium-catalyzed enantiodivergent synthesis of C–N axially chiral biaryls. *J. Am. Chem. Soc.* **145**, 8417–8429 (2023).
77. Q. Tian, J. Ge, Y. Liu, X. Wu, Z. Li, G. Cheng, Solvent-controlled enantiodivergent construction of P(V)-stereogenic molecules via palladium-catalyzed annulation of prochiral N-Aryl phosphonamides with aromatic iodides. *Angew. Chem. Int. Ed. Engl.* **63**, e202409366 (2024).

78. M.-A. Abadie, X. Trivelli, F. Medina, N. Duhal, M. Kouach, B. Linden, E. Génin, M. Vandewalle, F. Capet, P. Roussel, I. D. Rosal, L. Maron, F. Agbossou-Niedercorn, C. Michon, Gold(I)-catalysed asymmetric hydroamination of alkenes: A silver- and solvent-dependent enantiodivergent reaction. *Chem. A Eur. J.* **23**, 10777–10788 (2017).
79. F. Wang, J. Jing, Y. Zhao, X. Zhu, X. Zhang, L. Zhao, P. Hu, W.-Q. Deng, X. Li, Rhodium-catalyzed C−H activation-based construction of axially and centrally chiral indenes through two discrete insertions. *Angew. Chem. Int. Ed. Engl.* **60**, 16628–16633 (2021).
80. S. Zhang, Q. Zhang, M. Tang, Synthesis of hydrazides from *N*-tosylhydrazones and its application in the preparation of indazolones. *J. Org. Chem.* **87**, 3845–3850 (2022).
81. M. J. Frisch, G. W. Trucks, H. B. Schlegel, G. E. Scuseria, M. A. Robb, J. R. Cheeseman, G. Scalmani, V. Barone, G. A. Petersson, H. Nakatsuji, X. Li, M. Caricato, A. V. Marenich, J. Bloino, B. G. Janesko, R. Gomperts, B. Mennucci, H. P. Hratchian, J. V. Ortiz, A. F. Izmaylov, J. L. Sonnenberg, D. Williams-Young, F. Ding, F. Lipparini, F. Egidi, J. Goings, B. Peng, A. Petrone, T. Henderson, D. Ranasinghe, V. G. Zakrzewski, J. Gao, N. Rega, G. Zheng, W. Liang, M. Hada, M. Ehara, K. Toyota, R. Fukuda, J. Hasegawa, M. Ishida, T. Nakajima, Y. Honda, O. Kitao, H. Nakai, T. Vreven, K. Throssell, J. A. Montgomery Jr., J. E. Peralta, F. Ogliaro, M. J. Bearpark, J. J. Heyd, E. N. Brothers, K. N. Kudin, V. N. Staroverov, T. A. Keith, R. Kobayashi, J. Normand, K. Raghavachari, A. P. Rendell, J. C. Burant, S. S. Iyengar, J. Tomasi, M. Cossi, J. M. Millam, M. Klene, C. Adamo, R. Cammi, J. W. Ochterski, R. L. Martin, K. Morokuma, O. Farkas, J. B. Foresman, D. J. Fox, Gaussian 16, Revision A. 03 (Gaussian Inc., 2016).
82. C. Lee, W. Yang, R. G. Parr, Development of the Colle-Salvetti correlation-energy formula into a functional of the electron density. *Phys. Rev. B: Condens. Matter* **37**, 785–789 (1988).
83. A. D. Becke, Density-functional thermochemistry. III. The role of exact exchange. *J. Chem. Phys.* **98**, 5648–5652 (1993).
84. S. Grimme, J. Antony, S. Ehrlich, H. Krieg, A consistent and accurate ab initio parametrization of density functional dispersion correction (DFT-D) for the 94 elements H-Pu. *J. Chem. Phys.* **132**, 154104 (2010).
85. S. Grimme, S. Ehrlich, L. Goerigk, Effect of the damping function in dispersion corrected density functional theory. *J. Comput. Chem.* **32**, 1456–1465 (2011).
86. F. Weigend, R. Ahlrichs, Balanced basis sets of split valence, triple zeta valence and quadruple zeta valence quality for H to Rn: Design and assessment of accuracy. *Phys. Chem. Chem. Phys.* **7**, 3297–3305 (2005).
87. F. Weigend, Accurate Coulomb-fitting basis sets for H to Rn. *Phys. Chem. Chem. Phys.* **8**, 1057–1065 (2006).
88. Y. Zhao, D. G. Truhlar, The M06 suite of density functionals for main group thermochemistry, thermochemical kinetics, noncovalent interactions, excited states, and transition elements: Two new functionals and systematic testing of four M06-class functionals and 12 other functionals. *Theor. Chem. Acc.* **120**, 215–241 (2008).
89. A. V. Marenich, C. J. Cramer, D. G. Truhlar, Universal solvation model based on solute electron density and a continuum model of the solvent defined by the bulk dielectric constant and atomic surface tensions. *J. Phys. Chem. B* **113**, 6378–6396 (2009).
90. C. Y. Legault, CYLview20 (Université de Sherbrooke, 2020); (www.cylview.org).
91. D. H. Wertz, Relationship between the gas-phase entropies of molecules and their entropies of solvation in water and 1-octanol. *J. Am. Chem. Soc.* **102**, 5316–5322 (1980).
92. B. O. Leung, D. L. Reid, D. A. Armstrong, A. Rauk, Entropies in solution from entropies in the gas phase. *J. Phys. Chem. A* **108**, 2720–2725 (2004).
93. R. L. Martin, P. J. Hay, L. R. Pratt, Hydrolysis of ferric ion in water and conformational equilibrium. *J. Phys. Chem. A* **102**, 3565–3573 (1998).
94. H. Li, J. Jiang, G. Lu, F. Huang, Z.-X. Wang, On the "reverse gear" mechanism of the reversible dehydrogenation/hydrogenation of a nitrogen heterocycle catalyzed by a Cp*Ir complex: A computational study. *Organometallics* **30**, 3131–3141 (2011).
95. H. Li, M. Wen, Z.-X. Wang, computational mechanistic study of the hydrogenation of carbonate to methanol catalyzed by the Ru^{II}PNN complex. *Inorg. Chem.* **51**, 5716–5727 (2012).
96. M. Wen, F. Huang, G. Lu, Z.-X. Wang, Density functional theory mechanistic study of the reduction of CO_2 to CH_4 catalyzed by an ammonium hydridoborate ion pair: CO_2 activation via formation of a formic acid entity. *Inorg. Chem.* **52**, 12098–12107 (2013).
97. S. Qu, Y. Dang, C. Song, M. Wen, K.-W. Huang, Z.-X. Wang, Catalytic mechanisms of direct pyrrole synthesis via dehydrogenative coupling mediated by PNP-Ir or PNN-Ru pincer complexes: Crucial role of proton-transfer shuttles in the PNP-Ir system. *J. Am. Chem. Soc.* **136**, 4974–4991 (2014).
98. G. H. Zimmerman, R. H. Wood, Conductance of dilute sodium acetate solutions to 469 K and of acetic acid and sodium acetate/acetic acid mixtures to 548 K and 20 MPa. *J. Solut. Chem.* **31**, 995–1017 (2002).

Acknowledgments

Funding: Financial support for this work was provided by the following agencies: National Key R&D Program of China (2022YFA1503104 to X.-X.L.), National Natural Science Foundation of China (nos. 22371175, 22101167, 22122109, and 22271253), National Key R&D Program of China (2022YFA1504301 to X.H.), Zhejiang Provincial Natural Science Foundation of China (grant no. LDQ23B020002 to X.H.), the Starry Night Science Fund of Zhejiang University Shanghai Institute for Advanced Study (SN-ZJU-SIAS-006 to X.H.), Beijing National Laboratory for Molecular Sciences (BNLMS202102 to X.H.), CAS Youth Interdisciplinary Team (JCTD-2021-11 to X.H.), Fundamental Research Funds for the Central Universities (226-2022-00140, 226-2022-00224, and 226-2023-00115 to X.H.), the State Key Laboratory of Clean Energy Utilization (ZJUCEU2020007 to X.H.), and the Leading Innovation Team grant from Department of Science and Technology of Zhejiang Province (2022R01005 to X.H.). **Author contributions:** Conceptualization: X.L. Methodology: R.M. Investigation: R.M. Mechanistic studies by DFT calculations: X.H., X.-X.L. and R.W. Writing—original draft: J.J., F.W., and X.L. **Competing interests:** The authors declare that they have no competing interests. **Data and materials availability:** All data needed to evaluate the conclusions in the paper are present in the paper and/or the Supplementary Materials.

Submitted 1 July 2024
Accepted 24 October 2024
Published 27 November 2024
10.1126/sciadv.adr4435